ECCOMAS Congress 2016
VII European Congress on Computational Methods in Applied Sciences and Engineering
M. Papadrakakis, V. Papadopoulos, G. Stefanou, V. Plevris (eds.)
Crete Island, Greece, 5–10 June 2016

MODELING OF LOW-ALLOYED TRIP-STEELS BASED ON DIRECT MICRO-MACRO SIMULATIONS

S. Prüger[1], A. Gandhi[1], and D. Balzani[1,2]

[1]TU Dresden
Faculty of Civil Engineering
Institute of Mechanics and Shell Structures
01062 Dresden, Germany
e-mail: stefan.prueger,ashutosh.gandhi,daniel.balzani@tu-dresden.de

[2] Dresden Center for Computational Materials Science, Germany

Keywords: Computational homogenization, Low-alloyed TRIP-steel, Martensitic phase transformation, Transformation kinetics

Abstract. *Low-alloyed TRIP steels are often used in the automotive industry due to their favorable mechanical properties such as high ductility and strength and their moderate production costs. These steels possess a heterogeneous multiphase microstructure, initially consisting of ferrite, bainite and retained austenite which is responsible for the mechanical properties. Upon deformation, a diffusionless, stress-induced, martensitic phase transformation from austenite to martensite is observed, enhancing ductility and strength.*
*We focus on multi-scale methods in the sense of FE^2 to describe the macroscopic behavior of low-alloyed TRIP-steels, because this approach allows for a straightforward inclusion of various influencing factors such as residual stress distribution, graded material properties which can hardly included in phenomenological descriptions of these heterogeneous multiphase materials. In order to allow for efficient computations, a simplified microstructure is used in an illustrative direct micro-macro simulation. The inelastic processes in the austenitic inclusions involve the phase transformation from austenite to martensite and the inelastic deformation of these two phases. The isotropic, rate-independent, hyperelastic-plastic material model of Hallberg et al. (IJP, **23**, pp.1213–1239, 2007), originally proposed for high-alloyed TRIP steel, is adopted here for the inclusion phase. Minor modifications of the model are proposed to improve its implementation and performance. The influence of various material parameters associated with the phase transformation on the evolution of retained austenite is studied for different homogeneous deformation states. The non-monotonic stress-state dependence observed in experiments is clearly captured by the model. A numerical two-scale calculation is carried out to enlighten the ductility enhancement in low-alloyed TRIP-steels due to the martensitic phase transformation.*

1 INTRODUCTION

Low-alloyed TRIP-steels offer a favorable combination of both high strength and pronounced ductility, leading to a high energy absorption capacity. This is desired especially for automotive applications, because it allows for light-weight and crashworthy constructions and therefore leads to safer and more efficient automobiles. These favorable mechanical properties can be achieved at lower costs compared to high-alloyed TRIP-steels, due to the reduced amount of alloying elements required. In contrast to high-alloyed, initially fully austenititc TRIP-steels, low-alloyed TRIP-steels possess a multiphase microstructure, consisting of ferrite, bainite and retained austenite. In order to obtain the favorable mechanical properties the microstructure is optimized by a sophisticated heat treatment procedure and a smart alloy design, cf. [1]. Micromechanical considerations [2] lead to the conclusion that the high ductility of these steels cannot be solely attributed to the deformation-induced martensitic phase transformation from the metastable, retained austenite to martensite, because its volume fraction is typically in the range of 10-15% and therefore simply too low. Therefore, the multiphase character of the microstructure is responsible for the pronounced ductility. However, the phase transformation in the retained austenite plays an important role in this type of steel as it dynamically influences the stress and strain partitioning between different phases during deformation [3, 4, 5] and delays microcracking [6], leading to composite type microstructure with adaptive properties. The rate of the austenite to martensite transformation depends on various factors: (i) ambient temperature cf. [7], (ii) stress-state cf. [8], (iii) austenite grain size and morphology [9], (iv) neighboring constituents [9].

A variety of constitutive models has been proposed for the description of the deformation and transformation behavior of low-alloyed TRIP-steels. Phenomenological approaches such as [10, 11, 12, 13] mainly focus on capturing the influences of temperature and stress-state on the transformation kinetics. They are mostly used in single scale (macroscopic) simulations due to their low computational costs. Modeling approaches that incorporate analytical homogenization schemes, like for instance [14, 15, 16, 17, 18, 20] are better suited to account for the strengthening effect of the evolving martensite and multiphase character of the microstructure. However, simplifying assumptions regarding the microstructure morphology and field fluctuations within the phases have to be made, which may lead to inaccurate assessment of failure initialization. Direct microstructural simulations allow for a straightforward incorporation of all of the above mentioned influencing factors (i)-(iv). However, they are computationally very demanding as the macroscopic constitutive response is obtained by the solution of microscopic boundary value problems for a suitable representative volume element. In the context of low-alloyed TRIP-steels a two-dimensional microstructural section [21] or artificial inclusion type microstructure [22] as well as polyhedral inclusions representing single crystalline phases [23] have been used as representative volume elements.

In the current contribution, we follow the direct micro-macro simulation approach as this framework is in general sufficient to study the above mentioned influencing factors on the phase transformation behavior of low-alloyed TRIP-steels. The paper is organized as follows. In section 2, the basic equations for the direct micro-macro scale transition are summarized, whereas in section 3 a suitable material model for the phase transformation from austenite to martensite is adopted from the literature. In section 4, the influence of model parameters on the phase transformation behavior is illustrated and the effective mechanical behavior of a simplified three-dimensional microstructure for low-alloyed TRIP-steel is presented. Section 5 summarizes the main findings.

2 DIRECT MICRO-MACRO SCALE TRANSITION

Employing the direct micro-macro scale transition approach enables the computation of effective, macroscopic material behavior for a representative volume element with arbitrary complex microstructure by means of the solution of microscopic boundary value problems and appropriate averaging schemes of the microscopic fields. Here, we focus on a purely mechanical setting and state the basic relations, required for the computations. According to Hill [24] the stress power per unit reference volume at the macroscopic scale, expressed in terms of average quantities, should be equal to the microscopic counterpart, yielding

$$\langle \boldsymbol{P} : \dot{\boldsymbol{F}} \rangle = \langle \boldsymbol{P} \rangle : \langle \dot{\boldsymbol{F}} \rangle \,, \tag{1}$$

where $\boldsymbol{P}$ denotes the 1st Piola-Kirchhoff stress tensor, $\dot{\boldsymbol{F}}$ is the material time derivative of the deformation gradient and the volume average over the reference configuration is defined as $\langle \cdot \rangle = \frac{1}{V} \int_{\mathcal{B}_0} \cdot \, \mathrm{d}V$. As the current study relies on representative volume elements with a periodic microstructure, it is convenient to apply periodic boundary conditions in order to enforce eq. (1). Based on the decomposition of the deformation field in a homogeneous deformation and fluctuation as

$$\dot{\boldsymbol{x}} = \dot{\overline{\boldsymbol{F}}} \cdot \boldsymbol{X} + \dot{\widetilde{\boldsymbol{w}}} \,, \tag{2}$$

the periodic boundary conditions require a periodic fluctuation field $\widetilde{\boldsymbol{w}}$ and antiperiodic traction vectors $\boldsymbol{t}_0$ along the boundary, namely

$$\dot{\widetilde{\boldsymbol{w}}}^{+} = \dot{\widetilde{\boldsymbol{w}}}^{-} \qquad \text{and} \qquad \boldsymbol{t}_0^{+} = -\boldsymbol{t}_0^{-} \text{ on } \partial\mathcal{B}_0 \,. \tag{3}$$

3 MATERIAL MODEL AT THE MICRO-SCALE

In order to obtain reliable predictions of the macroscopic, effective deformation and transformation behavior of low-alloyed TRIP-steels, suitable material models that capture the essential features of inelastic processes are required at micro-scale. The aim of the present contribution is to describe the overall behavior of low-alloyed TRIP-steels under isothermal conditions and excluding rate-dependent effects. Therefore, rate-independent models that incorporate the two main inelastic processes, plasticity and the austenite to martensite phase transformation, should be chosen. Furthermore, assuming a polycrystalline microstructure at the micro-scale, the constitutive model proposed by Hallberg [25] for high-alloyed TRIP-steels is a suitable choice, because it is contains only a relatively small number of material parameters, but still includes plasticity and phase transformation as two independently evolving inelastic processes and their interaction in a simplified manner. In contrast to the originally proposed model, we apply some minor modifications which allow for a more convenient implementation, but the essential features of the model remain and in particular the thermodynamic consistency is still guaranteed. The material model is based on the multiplicative split of the deformation gradient

$$\boldsymbol{F} = \boldsymbol{F}^{\mathrm{e}} \cdot \boldsymbol{F}^{\mathrm{in}} \tag{4}$$

into an elastic and an inelastic part where the latter is associated with any inelastic process occurring in the material. Employing the assumption of isotropic elastic behavior and an additive split of the free energy according to

$$\rho_0 \Psi(\boldsymbol{b}^{\mathrm{e}}, \alpha_1, \alpha_2, \ldots) = \rho_0 \Psi^{\mathrm{e}}(\boldsymbol{b}^{\mathrm{e}}) + \rho_0 \Psi^{\mathrm{in}}(\alpha_1, \alpha_2, \ldots) \,, \tag{5}$$

with α_i representing the internal variables, the Kirchhoff-stress is defined as

$$\boldsymbol{\tau} = 2\rho_0 \frac{\partial \Psi}{\partial \boldsymbol{b}^{\mathrm{e}}} \cdot \boldsymbol{b}^{\mathrm{e}} \,. \tag{6}$$

Herein, the elastic left Cauchy-Green tensor is given as $\boldsymbol{b}^{\mathrm{e}} = \boldsymbol{F}^{\mathrm{e}} \cdot \boldsymbol{F}^{\mathrm{e}T}$. In particular, the elastic energy function

$$\rho_0 \Psi^{\mathrm{e}} = \frac{\lambda}{2} \left[\sum_A \ln(\lambda_A^{\mathrm{e}}) \right]^2 + \mu \sum_A \left[\ln(\lambda_A^{\mathrm{e}}) \right]^2 \tag{7}$$

is utilized, which is described in terms of principle elastic stretches λ_A^{e} and the Lamé constants λ, μ. The principle elastic stretches are obtained by the eigenvalue decomposition of $\boldsymbol{b}^{\mathrm{e}}$. The elastic left Cauchy-Green tensor can be related to the inelastic right Cauchy-Green tensor $\boldsymbol{C}^{\mathbf{in}} = \boldsymbol{F}^{\mathbf{in}T} \cdot \boldsymbol{F}^{\mathbf{in}}$ via

$$\boldsymbol{b}^{\mathrm{e}} = \boldsymbol{F} \cdot \boldsymbol{C}^{\mathbf{in}^{-1}} \cdot \boldsymbol{F}^T \,, \tag{8}$$

whereas the temporal evolution of $\boldsymbol{b}^{\mathrm{e}}$ and $\boldsymbol{C}^{\mathbf{in}}$ is expressed as

$$\mathcal{L}(\boldsymbol{b}^{\mathrm{e}}) = \boldsymbol{F} \cdot \left(\boldsymbol{C}^{\mathbf{in}^{-1}} \right)^{\cdot} \cdot \boldsymbol{F}^T \tag{9}$$

where $\mathcal{L}$ is the Lie derivative. An alternative representation of eq. (9) solely in terms of $\boldsymbol{C}^{\mathbf{in}}$ and $\boldsymbol{F}$ is obtained if the additive split of the rate of deformation $\boldsymbol{l} = \dot{\boldsymbol{F}} \cdot \boldsymbol{F}^{-1} = \boldsymbol{l}^{\mathrm{e}} + \boldsymbol{l}^{\mathbf{in}}$ is used in conjunction with the assumption of isotropic elastic and inelastic behavior, which is considered here, i.e.

$$\left(\boldsymbol{C}^{\mathbf{in}^{-1}} \right)^{\cdot} = -2\boldsymbol{F}^{-1} \cdot \underbrace{\sum_p \dot{\lambda}_p \frac{\partial \Phi_p}{\partial \boldsymbol{\tau}}}_{=\boldsymbol{d}^{\mathbf{in}}} \cdot \boldsymbol{F} \cdot \boldsymbol{C}^{\mathbf{in}^{-1}} \,. \tag{10}$$

As proposed by Hallberg [25] the inelastic rate of deformation $\boldsymbol{d}^{\mathbf{in}}$ is additively split into multiple contributions stemming from different inelastic processes, characterized by independent limit surfaces Φ_p and the corresponding consistency parameters $\dot{\lambda}_p$. Similar to small strain elastic-plastic formulations, the antimetric part of the inelastic velocity gradient remains undetermined.

For the rate-independent plasticity a limit surface of VON MISES-type with nonlinear isotropic hardening is chosen.

$$\Phi^{\mathrm{pl}} := \sqrt{3J_2} - \sigma^{\mathrm{y}}(\alpha^{\mathrm{pl}}, f_{\mathrm{m}}) \tag{11}$$

Herein the second invariant of the Kirchhoff stress deviator is defined as $J_2 = \frac{1}{2}\mathrm{dev}(\boldsymbol{\tau}) : \mathrm{dev}(\boldsymbol{\tau})$, whereas α^{pl} and f_{m} are the isotropic hardening variable and the martensite volume fraction, respectively. The yield stress is computed from an exponential hardening law and a nonlinear rule of mixture, according to

$$\sigma^{\mathrm{y}}(\alpha^{\mathrm{pl}}, f_{\mathrm{m}}) = \sigma_0^{\mathrm{y}} \bar{m}(f_{\mathrm{m}}) + \mathrm{H}\kappa(\alpha^{\mathrm{pl}}) \tag{12}$$

with

$$\bar{m}(f_{\mathrm{m}}) = 1 + (\exp(\mathrm{f}_1 f_{\mathrm{m}}) - 1)\mathrm{f}_2 \tag{13}$$

and

$$\kappa(\alpha^{\mathrm{pl}}) = \frac{\mathrm{R}_\infty}{\mathrm{H}} \left[1 - \exp\left(-\frac{\mathrm{H}}{\mathrm{R}_\infty} \alpha^{\mathrm{pl}} \right) \right] \,, \tag{14}$$

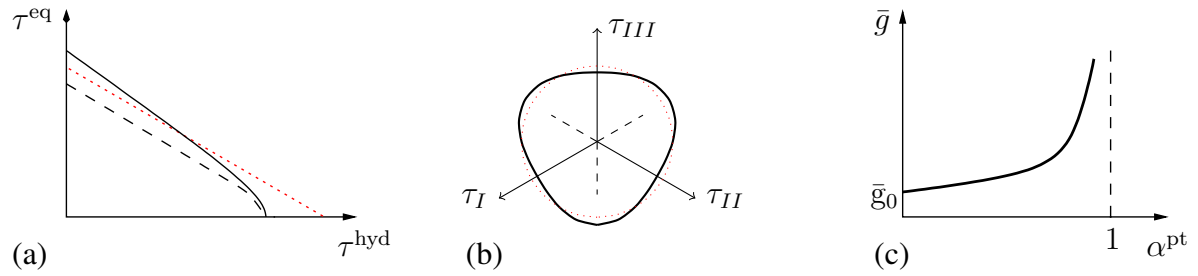

Figure 1: Limit surface for phase transformation: (a) section containing the hydrostatic axis with tensile $(--)$ and compressive meridian $(—)$ and the corresponding cone $(\cdots)$, (b) non-circular cross-section in the π-plane, (c) evolution of the transformation barrier.

where the hardening variable evolves according to $\dot{\alpha}^{\mathrm{pl}} = \dot{\lambda}^{\mathrm{pl}}$. The equations (12), (13), (14) introduce three material parameters $(\sigma_0^{\mathrm{y}}, \mathrm{H}, \mathrm{R}_\infty)$ for the hardening and two material parameters $(\mathrm{f}_1, \mathrm{f}_2)$ in the rule of mixture.
The limit surface for phase transformation is taken here as a hyperbolic approximation of Hallberg's conical transformation surface and is inspired by the proposal given in [26]. It possesses the form

$$\Phi^{\mathrm{pt}} := \sqrt{(\tau^{\mathrm{eq}})^2 \left(1 + \mathrm{k}\frac{J_3}{J_2^{3/2}}\right)^2 \mathrm{R}^2 + \Delta_{\mathrm{v}}^2(\kappa_1^2(\alpha^{\mathrm{pt}}, T) - 1)(\tau^{\mathrm{hyd}})^2 + \Delta_v \kappa_2(\alpha^{\mathrm{pt}}, T)\tau^{\mathrm{hyd}} - \mathrm{R}\kappa_1(\alpha^{\mathrm{pt}}, T)}\,, \quad (15)$$

with

$$\kappa_1(\alpha^{\mathrm{pt}}, T) = \sqrt{\left(\frac{1}{\Delta_{\mathrm{v}}}\left(\bar{g}(\alpha^{\mathrm{pt}}) - \Delta g^{\mathrm{a}\to\mathrm{m}}(T)\right)\right)^2 - \mathrm{c}^2} \quad (16)$$

$$\kappa_2(\alpha^{\mathrm{pt}}, T) = \frac{1}{\Delta_{\mathrm{v}}}\frac{\bar{g}(\alpha^{\mathrm{pt}}) - \Delta g^{\mathrm{a}\to\mathrm{m}}(T)}{\kappa_1}\,. \quad (17)$$

The transformation surface introduces the material parameters $\Delta_{\mathrm{v}}, \mathrm{R}$ which correspond to the volumetric and deviatoric transformation strain, as well as the shape parameters k and c. The parameter k controls the deviation from the circular cross-section in the π-plane, i.e. the deviatoric plane that contains the origin and the parameter c determines the transition from the hyperbolic surface to the conical surface (see fig. 1). The latter parameter, however, is of minor importance in the studies considered in this paper. Although it guarantees a continuous differentiable limit surface under purely hydrostatic loading conditions, for the stress states reached in the loading scenarios considered, the hyperbolic approximation of the transformation surface is very close to the original conical surface. Furthermore, $\tau^{\mathrm{hyd}}, \tau^{\mathrm{eq}}, \Delta g^{\mathrm{a}\to\mathrm{m}}(T)$ and $\bar{g}(\alpha^{\mathrm{pt}})$ denote the hydrostatic part of the Kirchhoff stress, the VON MISES equivalent Kirchhoff stress, the temperature dependent energy difference between the austenitic (a) and the martensitic (m) phase and the transformation barrier, respectively. The evolution equations for the internal variables associated with the transformation, namely the hardening variable for transformation hardening $\alpha_1 := \alpha^{\mathrm{pt}}$ and the martensite volume fraction $\alpha_2 := f_{\mathrm{m}}$ are derived following the procedure for generalized standard materials [27]. Therefore, the portion of the free energy function corresponding to inelastic processes, introduced in eq. (5), is further specified as

$$\rho_0\Psi^{\mathrm{in}}(\alpha^{\mathrm{pt}}, \alpha^{\mathrm{pl}}, f_{\mathrm{m}}) = \rho_0\Psi^{\mathrm{pl}}(\alpha^{\mathrm{pl}}) + \rho_0\Psi^{\mathrm{pt}}(\alpha^{\mathrm{pt}}) + \rho_0\Psi^{\mathrm{chem}}(f_{\mathrm{m}}; T) \quad (18)$$

with

$$\rho_0\Psi^{\mathrm{chem}}(f_{\mathrm{m}}; T) = (1 - f_{\mathrm{m}})\rho_0\Psi_{\mathrm{a}}^{\mathrm{chem}}(T) + f_{\mathrm{m}}\rho_0\Psi_{\mathrm{m}}^{\mathrm{chem}}(T) \quad (19)$$

and

$$\rho_0 \Psi^{\mathrm{pt}}(\alpha^{\mathrm{pt}}) = \bar{\mathrm{g}}_1 \left(\left(1 - \alpha^{\mathrm{pt}}\right) \left(\ln(1 - \alpha^{\mathrm{pt}}) - 1 \right) + 1 \right) . \tag{20}$$

Herein, $\Psi^{\mathrm{pl}}(\alpha^{\mathrm{pl}})$ is linked to the isotropic hardening of the VON MISES criterion and chosen identical to the proposal of Hallberg [25] and is not included here for brevity. Upon defining the driving forces $K_{\alpha^{\mathrm{pt}}} = \rho_0 \frac{\partial \Psi^{\mathrm{pt}}}{\partial \alpha^{\mathrm{pt}}}$ and $K_{f_{\mathrm{m}}} = \rho_0 \frac{\partial \Psi^{\mathrm{chem}}}{\partial f_{\mathrm{m}}} = -\Delta g^{\mathrm{a}\to\mathrm{m}}(T)$, the evolution equations are defined as

$$\dot{f_{\mathrm{m}}} = -\dot{\lambda}^{\mathrm{pt}} \frac{\partial \Phi^{\mathrm{pt}}}{\partial K_{f_{\mathrm{m}}}} \tag{21}$$

$$\dot{\alpha}^{\mathrm{pt}} = -\dot{\lambda}^{\mathrm{pt}} \frac{\partial \Phi^{\mathrm{pt}}}{\partial K_{\alpha^{\mathrm{pt}}}} . \tag{22}$$

From the structure of the transformation surface it can be readily verified that $\alpha^{\mathrm{pt}} = f_{\mathrm{m}}$. The transformation barrier evolves according to the transformation hardening law

$$\bar{g}(\alpha^{\mathrm{pt}}) = \bar{\mathrm{g}}_0 - \bar{\mathrm{g}}_1 \ln(1 - \alpha^{\mathrm{pt}}) \tag{23}$$

with the initial transformation barrier $\bar{\mathrm{g}}_0$ and the initial hardening modulus $\bar{\mathrm{g}}_1$. As can be seen from fig. 1c the barrier is progressively increasing, limiting the hardening variable to $\alpha^{\mathrm{pt}} \leq 1$. The material model described above is implemented into the Finite Element Program FEAP and employs a combination of the operator split and a general return mapping algorithm proposed by Aurrichio et al. [28] to integrate the set of nonlinear evolution equations. Furthermore, the return mapping algorithm has been extended to handle non-smooth intersections of multiple limit surfaces as discussed in [29, p.206ff].

4 RESULTS

4.1 Parameter study

The material model described in section 3 contains 12 material parameters, which need to be adjusted in order to capture the deformation and transformation behavior of the retained austenite and the evolving martensite. The parameters associated with elasticity and plasticity of the austenitic/martensitic material can be chosen rather easily, if the individual hardening curves are known. In the present paper the parameters are set such that the austenite and martensite hardening curves of an experimental TRIP-steel presented in [19] are reproduced. For later reference they are listed in table 1. The influence of three of the remaining parameters, namely the

E [MPa]	ν	σ_0^{y} [MPa]	H [MPa]	R_∞[MPa]	f_1	f_2	Δ_{v}	R
200000	0.3	300	3500	420	1.65	1.1	0.04	0.07

Table 1: Material parameters of the austenitic/martensitic material

initial transformation barrier $\bar{\mathrm{g}}_0$, the initial transformation hardening modulus $\bar{\mathrm{g}}_1$ and the shape parameter k is studied in order to get a reasonable estimate for the range of parameters and their impact on the transformation kinetics. It is well known from experiments that the phase transformation in low-alloyed TRIP-steels is stress-state dependent. In particular, this dependence is non-monotonic with respect to the stress-triaxiality measure $h = \frac{\tau^{\mathrm{hyd}}}{\tau^{\mathrm{eq}}}$, based on the experimental results presented in [8] and depicted in fig.2c. Herein, 4 mechanical tests (simple shear, uniaxial tension, biaxial tension and the Marchiniak test) are carried out, where each of

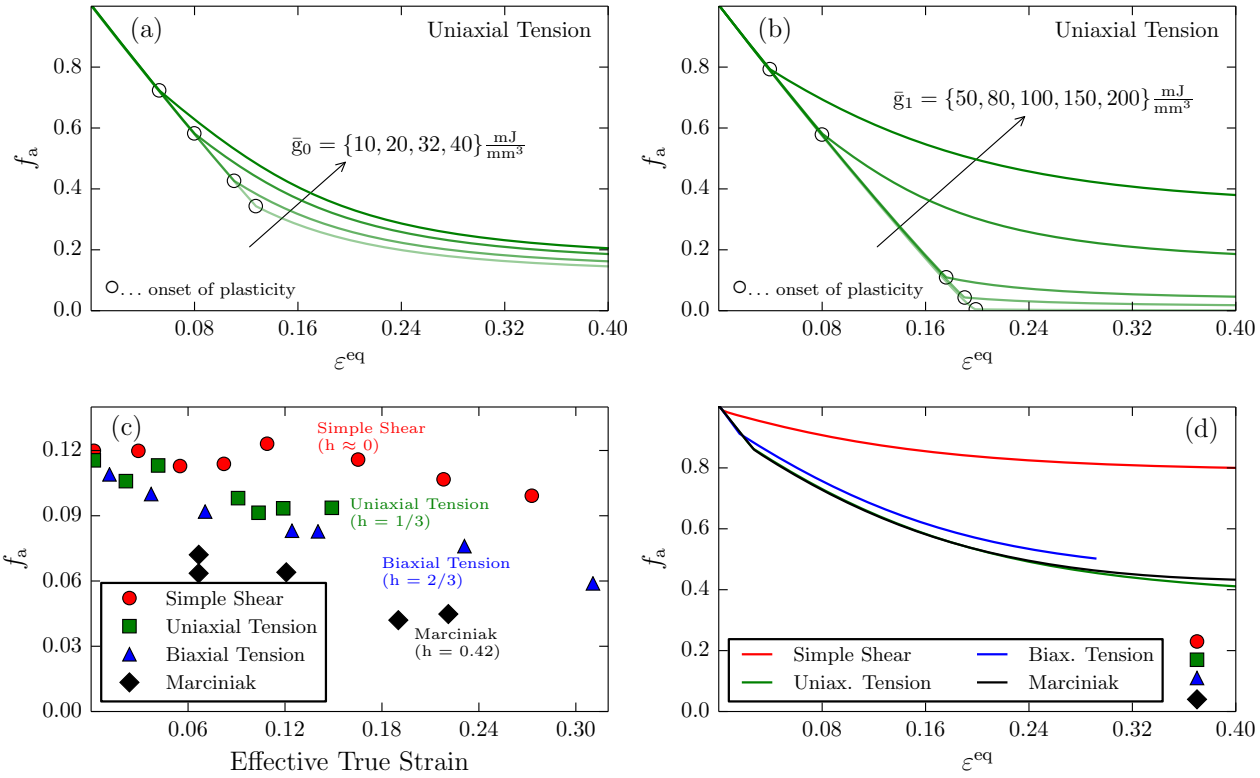

Figure 2: Influence on transformation kinetics: (a) variation of initial transformation barrier, (b) variation of transformation hardening modulus, (c) experimentally determined non-monotonic stress-state dependence cf. [8], (d) simulated non-monotonic stress-state dependence (symbols indicate the experimental trends: lowest transformation rate in simple shear and highest rate in Marciniak test)

these tests is characterized by a different stress state. These four tests are simulated employing deformation controlled one element tests with an initially fully austenitic microstructure and analyzing the evolution of retained austenite as a function of the overall equivalent strain ε^{eq}. It can be seen from fig. 2a,b that initially only phase transformation and no plastic deformation is predicted by the model for the given choice of parameters. While varying the initial transformation barrier changes the onset of plasticity, i.e. both inelastic deformation mechanisms are active at the same time and keeps the asymptotically reached value of retained austenite more or less unaltered, a modification of the hardening modulus influences both the onset of plasticity and the asymptotically reached value of retained austenite. In both studies a value of k=0.24 and $\bar{g}_1 = 150 \frac{mJ}{mm^3}$ and $\bar{g}_0 = 32 \frac{mJ}{mm^3}$ is kept while varying the other parameters. Although only the results for the uniaxial tensile test are presented, the same trend can be observed for all the homogeneous tests.

In a third study the shape parameter k is altered in the range of $-0.24 \leq k \leq 0.24$ leading to convex, non-circular cross-sections of the transformation in the π-plane. The initial transformation barrier and the transformation hardening are chosen in this study as $\bar{g}_0 = 40 \frac{mJ}{mm^3}$ and $\bar{g}_1 = 200 \frac{mJ}{mm^3}$. It can be seen from fig. 2d that the non-monotonic stress-state dependency is clearly captured for the choice k$= 0.24$, as the transformation rate in biaxial tension ($h = 2/3$) is lower than in the Marciniak test ($h = 0.42$). However, the transformation rate predicted by the material model in uniaxial tension contradicts the experimentally observed trend, which indicates the need for further parameter studies. For lower values of k the highest rate of transformation is observed in biaxial tension, leading to a proportional increase in transformation rate with increasing stress triaxiality.

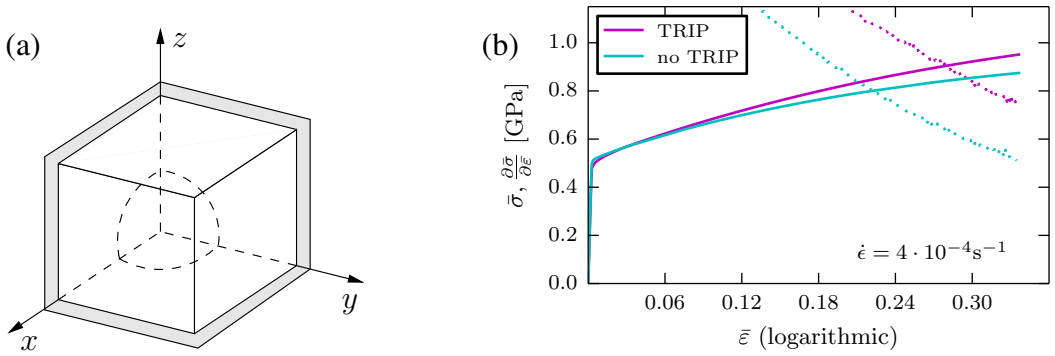

Figure 3: Simplified microstructure (a) and overall true stress-strain curve for uniaxial tension (b)

4.2 Simplified microstructure

In order to study the influence of the martensitic phase transformation on the macroscopic deformation behavior of low-alloyed TRIP-steels a simplified microstructure is considered which consists of a regular cubic arrangement of spherical, retained austenite inclusions embedded in ferritic/bainitic matrix. Note that more sophisticated but still efficient statistically similar representative volume elements may be constructed following the approach in Balzani et al. [30], see also Brands et al. [31] for an analysis in the context of DP steels. Consistent with experimental data, the initial volume fraction of retained austenite is chosen $f_{\mathrm{a}} = 0.12$. In the matrix a mixture of ferrite and bainite is employed with the volume fractions set to $f_{\mathrm{f}} = 0.5$ and $f_{\mathrm{b}} = 0.38$, corresponding to the phase composition of an experimental TRIP-steel presented in [19]. Both in the matrix and in the inclusion the material model described in section 3 is utilized. In the inclusion the material parameters given in table 1 and $\bar{\mathrm{g}}_0 = 40 \frac{\mathrm{mJ}}{\mathrm{mm}^3}$, $\bar{\mathrm{g}}_1 = 200 \frac{\mathrm{mJ}}{\mathrm{mm}^3}$ and k$= 0.24$ have been selected. As no phase transformation is observed in the matrix a rather high initial transformation barrier is used to switch off the transformation criterion. The material parameters associated with the nonlinear hardening law are computed to reasonable approximate the ferrite and bainite hardening curves given in [19]. All the material parameters required for the ferrite/bainite mixture are listed in table 2.
The representative volume element (RVE) containing the simplified microstructure is subjected to a displacement controlled uniaxial tensile test prescribing an axial true strain of $\bar{\varepsilon} = 0.34$. Due to the symmetry intrinsic to the boundary value problem, only $1/8$ of the RVE as depicted

$\mathrm{E}_{\mathrm{Matr}}$ [MPa]	ν_{Matr}	$\sigma^{\mathrm{y}}_{0,\mathrm{Matr}}$ [MPa]	H [MPa]	$\mathrm{R}_{\infty,\mathrm{Matr}}$[MPa]	$\mathrm{f}_{1,\mathrm{Matr}}$	$\mathrm{f}_{2,\mathrm{Matr}}$
200000	0.3	548	1800	550	1.65	1.1

Table 2: Material parameters for the ferritic/bainitic matrix

in fig. 3a is simulated. The overall true stress-strain curve is shown in fig. 3b for the cases of a transforming and a non-transforming retained austenite inclusion. The latter case corresponds to conditions of higher ambient temperatures where the retained austenite is stabilized leading to negligible transformation rates. Although the increase in the overall stress due to transformation is less than 100 MPa, the ductility is enhanced substantially ($+0.05$ true strain). The Considère criterion is employed as a measure of ductility, which estimates the limit of uniform elongation under uniaxial tension by the intersection of the flow curve and the instantaneous hardening modulus, i.e. $\bar{\sigma} = \frac{\partial \bar{\sigma}}{\partial \bar{\varepsilon}}$. The increase in ductility cannot be attributed solely to the transformation strains, but rather to the change in the yield behavior, because the inclusion has only transformed partly (see fig. 3b), indicating a dynamic stress and strain redistribution during

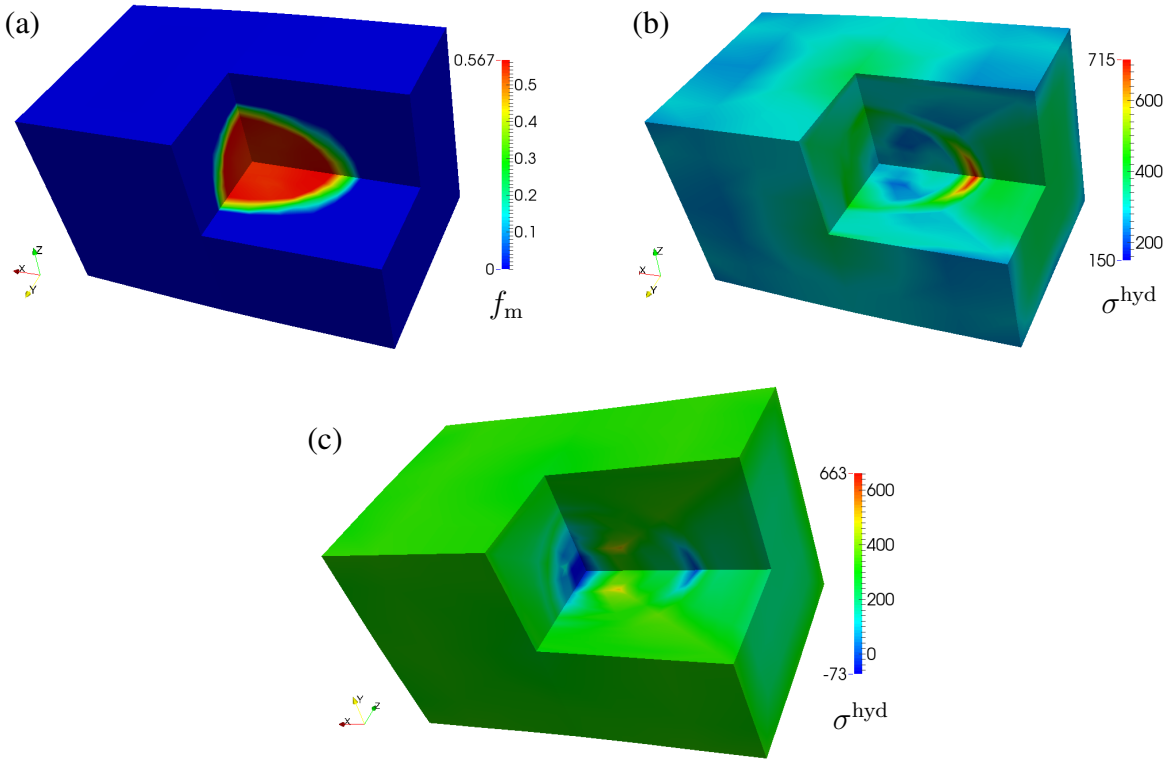

Figure 4: Distribution of martensite volume fraction (a) and hydrostatic Cauchy stress: (b) with and (c) without a→m transformation at the micro-scale under macroscopic uniaxial tension ($\bar{\varepsilon} = 0.34$)

loading.

Also on the micro-scale, significantly different stress distributions are obtained. Comparing fig. 4b and c, one observes higher hydrostatic stresses in the matrix close to the transforming inclusion, revealing a potential location of ductile damage initiation, which is absent in the microstructure with non-transforming retained austenite. Here the highest hydrostatic stress is observed in the inclusion.

5 CONCLUSIONS

In this contribution a simple material model for the austenite to martensite phase transformation in high-alloyed TRIP-steels is adopted for the direct micro-macro simulation of multiphase, low-alloyed TRIP-steels. Minor modifications of the model are proposed to improve its implementation and performance. A parameter study is conducted to illustrate the influence of material parameters, such as the initial transformation barrier, transformation hardening modulus and a shape parameter of the transformation surface on the phase transformation kinetics under different homogeneous loading conditions. Comparing the simulated evolution of retained austenite to experiments, it is found that the non-monotonic stress-state dependence can be reproduced by the model. For a reasonable choice of the material parameters of the single phases, a direct micro-macro simulation of a low-alloyed TRIP-steel is carried out employing a simplified, periodic microstructure. It is observed that austenite to martensite phase transformation enhances the ductility through a dynamic stress and strain redistribution between the constituents.

REFERENCES

[1] P.J. Jacques, *Phase transformation in transformation induced plasticity (TRIP)-assisted multiphase steels, in: Phase Transformations in Steels, Vol. 2*. Woodhead Publishing, 2012.

[2] H.K.D.H. Bhadeshia, TRIP-assisted Steels?, *ISIJ International*, **42**, 1059-1060, 2002.

[3] P.J. Jacques, Transformation-induced plasticity for high strength formable steels, *Current Opinion in Solid State and Materials Science*, **8**, 259–265, 2004.

[4] O. Muránsky, P. Šittner, J. Zrník, E.C. Oliver, In situ neutron diffraction investigation of the collaborative deformation-transformation mechanism in TRIP-assisted steels at room and elevated temperatures, *Acta Materialia*, **56**, 3367–3379, 2008.

[5] R. Petrov, L. Kestens, A. Wasilkowska, Y. Houbaert, Microstructure and texture of a lightly deformed TRIP-assisted steel characterized by means of the EBSD technique, *Materials Science and Engineering: A*, **447**, 285–297, 2007.

[6] I. de Diego-Calderón, M.J. Santofimia, J.M. Molina-Aldareguia, M.A. Monclús, I. Sabirov, Deformation behavior of a high strength multiphase steel at macro- and micro-scales, *Materials Science and Engineering: A*, **611**, 201–211, 2014.

[7] M. Radu and J. Valy and A.F. Gourgues and F. Le Strat and A. Pineau, Continuous magnetic method for quantitative monitoring of martensitic transformation in steels containing metastable austenite, *Scripta Materialia*, **52**, 525–530, 2005.

[8] P.J. Jacques, Q. Furnémont, F. Lani, T. Pardoen, F. Delannay, Multiscale mechanics of TRIP-assisted multiphase steels: I. Characterization and mechanical testing, *Acta Materialia*, **55**, 3681–3693, 2007.

[9] A.F. Mark, X. Wang, E. Essadiqi, J.D. Embury, J.D. Boyd, Development and characterisation of model TRIP steel microstructures, *Materials Science and Engineering: A*, **576**, 108–117, 2013.

[10] G.N. Haidemenopoulos, N. Aravas, I. Bellas, Kinetics of strain-induced transformation of dispersed austenite in low-alloy TRIP steels, *Materials Science and Engineering: A*, **615**, 416–423, 2014.

[11] R. Mahnken, A. Schneidt, T. Antretter, Macro modelling and homogenization for transformation induced plasticity of a low-alloy steel, *International Journal of Plasticity*, **25**, 183–204, 2009.

[12] R. Mahnken, M. Wolff, A. Schneidt, M. Böhm, Multi-phase transformations at large strains Thermodynamic framework and simulation, *International Journal of Plasticity*, **39**, 1–26, 2012.

[13] M. Mukherjee, T. Bhattacharyya, S.B. Singh, Models for Austenite to Martensite Transformation in TRIP-Aided Steels: A Comparative Study, *Materials & Manufacturing Processes*, **25**, 206–210, 2010.

[14] W.J. Dan, W.G. Zhang, S.H. Li, Z.Q. Lin, Finite element simulation on strain-induced martensitic transformation effects in TRIP steel sheet forming, *Computational Materials Science*, **39**, 593–599, 2007.

[15] L. Delannay, P. Jacques, T. Pardoen, Modelling of the plastic flow of TRIP-aided multiphase steel based on an incremental mean-field approach, *International Journal of Solids and Structures*, **45**, 1825–1843, 2008.

[16] R.F. Kubler, M. Berveiller, P. Buessler, Semi phenomenological modelling of the behavior of TRIP steels, *International Journal of Plasticity*, **27**, 299–327, 2011.

[17] J.-Y. Liu, H. Lu, J.-M. Chen, J.-F. Jullien, T. Wu, Simulation of mechanical behavior of multiphase TRIP steel taking account of transformation-induced plasticity, *Computational Materials Science*, **43**, 646–654, 2008.

[18] I. Papatriantafillou, M. Agoras, N. Aravas, G. Haidemenopoulos, Constitutive modeling and finite element methods for TRIP steels, *Computational Methods in Applied Mechanics and Engineering*, **195**, 5094–5114, 2006.

[19] I.O. Papatriantafillou, *TRIP steels: constitutive modeling and computational issues*. PhD-thesis, 2005.

[20] T.K. Shan, S.H. Li, W.G. Zhang, Z.G. Xu, Prediction of martensitic transformation and deformation behavior in the TRIP steel sheet forming, *Materials & Design*, **29**, 1810–1816, 2008.

[21] K.S. Choi, W.N. Liu, X. Sun, M.A. Khaleel, Microstructure-based constitutive modeling of TRIP steel: Prediction of ductility and failure modes under different loading conditions, *Acta Materialia*, **57**, 2592–2604, 2009.

[22] R. Sierra, J.A. Nemes, Investigation of the mechanical behaviour of multi-phase TRIP steels using finite element methods, *International Journal of Mechanical Sciences*, **50**, 649–665, 2008.

[23] D.D. Tjahjanto, S. Turteltaub, A.S.J. Suiker, S. van der Zwaag, Transformation-induced plasticity in multiphase steels subjected to thermomechanical loading, *Philosophical Magazine*, **88**, 3369–3387, 2008.

[24] R. Hill, On constitutive macro-variables for heterogeneous solids at finite strain, *Proceedings of the Royal Society A*, **326**, 131–147, 1972.

[25] H. Hallberg, P. Håkansson, M. Ristinmaa, A constitutive model for the formation of martensite in austenitic steels under large strain plasticity, *International Journal of Plasticity*, **23**, 1213–1239, 2007.

[26] M. Budnitzki, M. Kuna, A thermomechanical constitutive model for phase transformations in silicon under pressure and contact loading conditions, *International Journal of Solids and Structures*, **49**, 1316–1324, 2012.

[27] J. Besson, G. Cailletaud, J.-L. Chaboche, S. Forest, *Non-Linear Mechanics of Materials*. Springer, 2010.

[28] F. Auricchio and R.L. Taylor, A return-map algorithm for general associative isotropic elasto-plastic materials in large deformation regimes, *International Journal of Plasticity*, **15**, 1999.

[29] J.C. Simo, T.J.R. Hughes, *Computational Inelasticity*. Springer, 1998.

[30] D. Balzani, L. Scheunemann, D. Brands, J. Schröder, Construction of two- and three-dimensional statistically similar RVEs for coupled micro-macro simulations, *Computational Mechanics*, **54**, 2014.

[31] D. Brands, D. Balzani, L. Scheunemann, J. Schröder, H. Richter, D. Raabe, Computational modeling of dual-phase steels based on representative three-dimensional microstructures obtained from EBSD data, *Archive of Applied Mechanics*, **86**, 2016.